

Synthesis and detailed characterization of bulk Sr₂PdO₃

Bessas, D.; Kantor, I.; Bourazani, D.; Georgalas, K.; Biniskos, N.; Zhang, L.; Dugulan, A. I.; Syskakis, E.

DOI

[10.1016/j.physb.2018.10.048](https://doi.org/10.1016/j.physb.2018.10.048)

Publication date

2019

Document Version

Final published version

Published in

Physica B: Condensed Matter

Citation (APA)

Bessas, D., Kantor, I., Bourazani, D., Georgalas, K., Biniskos, N., Zhang, L., Dugulan, A. I., & Syskakis, E. (2019). Synthesis and detailed characterization of bulk Sr₂PdO₃. *Physica B: Condensed Matter*, 554, 148-153. <https://doi.org/10.1016/j.physb.2018.10.048>

Important note

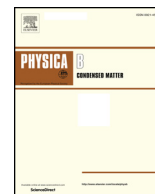
To cite this publication, please use the final published version (if applicable).
Please check the document version above.

Copyright

Other than for strictly personal use, it is not permitted to download, forward or distribute the text or part of it, without the consent of the author(s) and/or copyright holder(s), unless the work is under an open content license such as Creative Commons.

Takedown policy

Please contact us and provide details if you believe this document breaches copyrights.
We will remove access to the work immediately and investigate your claim.



Synthesis and detailed characterization of bulk Sr₂PdO₃

D. Bessas^{a,*}, I. Kantor^{b,1}, D. Bourazani^c, K. Georgalas^c, N. Biniskos^{d,e}, L. Zhang^f, A.I. Dugulan^a, E. Syskakis^c

^a *Fundamental Aspects of Materials and Energy, Department of Radiation Science and Technology, Delft University of Technology, Mekelweg 15, 2629 JB, Delft, the Netherlands*

^b *European Synchrotron Radiation Facility, F-38043, Grenoble, France*

^c *Section of Solid State Physics, Department of Physics, National and Kapodistrian University of Athens, GR-15784, Athens, Greece*

^d *Forschungszentrum Jülich GmbH, Jülich Centre for Neutron Science at ILL, 71 Avenue des Martyrs, 38000, Grenoble, France*

^e *Université Grenoble Alpes, CEA, INAC, MEM, 38000, Grenoble, France*

^f *BASF Nederland, NL-3454 PK, De Meern, the Netherlands*

ARTICLE INFO

Keywords:

4d transition metal oxide

Experimental study

Peculiar electronic properties

ABSTRACT

Bulk Sr₂PdO₃ was synthesized by a modified solid state reaction and a detailed characterization was carried out using both microscopic and macroscopic experimental techniques. Pd site exhibits an electric field gradient of $5.9(1) \cdot 10^{17}$ V/cm² due to the anisotropic local atomic configuration. A Curie - paramagnetic susceptibility indicating antiferromagnetic interactions superimposed to a core diamagnetic state is confirmed. A linear volume thermal expansion with a coefficient of $3.0(1) \cdot 10^{-5}$ K⁻¹ at room temperature is extracted. A collection of Einstein oscillators, with an Einstein temperature of about 115 K, is involved in the thermal transport. Large atomic displacements were observed in Sr vibrations. No Pd or Sr valence change is observed up to 900 K. A moderate anharmonicity is identified and quantified in a macroscopic Grüneisen parameter of 2.5(1) at room temperature. The electrical resistivity reveals a semiconducting behaviour. A systematic reduction in electrical resistivity and a change in the conduction mechanism is observed upon thermal cycling which indicates that a peculiar electronic mechanism is involved.

1. Introduction

Transition metal oxides containing 4d and 5d elements attract currently considerable attention not only for fundamental interest but also because they exhibit properties relevant to applications.

The search for materials which exhibit a superconducting transition at high temperatures was mainly focused in the past years in strongly correlated 3d transition metal containing systems [1]. The most studied systems in this respect are based on variations of the archetypal compound: La₂CuO₄ [2]. After the discovery of superconductivity in Sr₂RuO₄ [3] much attention was given in 4d and 5d transition metal containing oxide systems. Despite the coherent efforts only a few 4d and 5d transition metal based superconductors were found so far. Nevertheless, even if a transition to a superconducting state does not occur in such systems there are other interesting phenomena which may manifest. A characteristic example in this respect is Sr₂IrO₄ in which a superconducting ground state is expected [4], however, *only* a peculiar spin-orbit-induced insulating behaviour has been found [5].

Both the microscopic and macroscopic properties in 4d and 5d transition metal oxides are not as well understood as in 3d systems. The traditional Hund's rule, which takes into account only the spin degrees of freedom, fails to describe the magnetic state of such systems. In order to reproduce the experimental findings, strong correlations are usually taken into account [6] in theoretical studies. The spatial extent of the 4d and 5d electrons compared to the corresponding 3d is notably larger [7]. As a result an increased electronic d-orbital hopping is expected, electron-phonon coupling is of relevance, and strong lattice anharmonic effects, more enhanced compared to 3d transition metal oxides [8], may manifest in 4d and 5d transition metal containing oxides.

Sr₂PdO₃ exhibits an orthorhombic lattice structure (space group: *Immm*) and it is isostructural to both Sr₂CuO₃ [9] and Sr₂FeO₃ [10]. PdO₄ squares extend along the *b*-axis while the rest of the lattice is formed from SrO₇ polyhedra. The crystal structure of Sr₂PdO₃ is similar to the structure of the archetypal La₂CuO₄ high temperature superconductor. The only structural difference between Sr₂PdO₃ and La₂CuO₄ is an additional oxygen layer between the Pd ions along the *c*-

* Corresponding author. Present address: European Synchrotron Radiation Facility, F-38043, Grenoble, France.

E-mail address: bessas@esrf.fr (D. Bessas).

¹ Present address: Technical University of Denmark, Department of Physics, DK-2800 Lyngby, Denmark.

axis.

Sr_2PdO_3 has mainly been studied for its peculiar magnetic properties [11], which shows a core diamagnetic state superimposed to a Curie-paramagnetic behaviour. The phase equilibrium of Sr_2PdO_3 under pressure is also studied [12] and a structural transition is revealed at about 30 GPa. A transition to a superconducting state is not reported in Sr_2PdO_3 . Lately, the catalytic properties of Ca doped Sr_2PdO_3 towards a non-enzymatic glucose sensing were studied [13]. It was found that synergistic interactions between Sr (or Ca) and Pd lead to higher ionic and electronic conductivity and enhanced catalytic activity. It is, thus, interesting to study in more detail the local and the extended structure of Sr_2PdO_3 as well as the thermal, electrical, and vibrational properties in order to obtain a better insight in its functional properties.

In this study a combined microscopic and macroscopic experimental characterization of bulk Sr_2PdO_3 is carried out. The peculiar magnetic properties are confirmed. No indication of a structural transition is observed between 10 and 900 K. A collection of Einstein oscillators is involved in the thermal transport. A Grüneisen parameter of 2.5(1) is extracted at room temperature. A systematic reduction in electrical resistivity and a change in the conduction mechanism is observed upon thermal cycling which cannot be attributed to a valence change neither for Sr nor for Pd, which is 2+ up to 900 K.

2. Experimental methods

2.1. Sample synthesis

The synthesis of Sr_2PdO_3 was carried out by a modified solid state reaction. The starting materials were: a pure metallic Pd (5N) foil and $\text{Sr}(\text{NO}_3)_2$ powder. The Pd foil was first dissolved in excess HNO_3 in a silica tube, aided by a short rinse in aqua regia. The obtained solution was mixed with the appropriate amount of $\text{Sr}(\text{NO}_3)_2$ according to the required stoichiometry of the cations (2 Sr:1 Pd), in a highly dense Al_2O_3 crucible. The mixture was dried at 250 °C on a hot plate and a concomitant partial decomposition of nitrates occurred. The crucible was covered by a porous Al_2O_3 lid and heated up to 760 °C in air to complete the decomposition of the nitrates. The solid state reaction product was milled in an agate mortar, pelletized at 100 MPa, and preheated at 800 °C and 890 °C in air for 15 h, respectively, with a thorough intermediate grinding. To promote crystallization a final heating of the pellets was given at 1050 °C for 10 h in air, followed by an additional step at 1200 °C for 10 h under flowing O_2 .

2.2. Characterization

2.2.1. X-ray diffraction

The crystallographic phase purity and potential structural transitions were studied by temperature dependent powder diffraction between 10 and 300 K using Cu K_α radiation utilizing a calibrated Huber G670 image plate powder diffractometer, a standard Siemens D5000 powder diffractometer was used utilizing also Cu K_α radiation for the room temperature measurements, and synchrotron radiation, wavelength 0.4959(1) Å, was used at station BM23/ESRF between 300 and 900 K.

2.2.2. X-ray absorption

The valence and potential changes as well as the average of the instantaneous distance between the atomic pairs were studied by X-ray Absorption Spectroscopy (XAS) between 300 and 900 K. A double crystal fixed exit Si (1 1 1) monochromator was used to scan the energy around both the Sr and the Pd K-edges at 16.105 and 24.350 keV, respectively at station BM23/ESRF [14]. Two ionization chambers filled with a mixture of nitrogen and helium gases were used to measure the photon intensities before and after the sample.

The Sr K-edge and the Pd K-edge EXAFS data were extracted using

the Athena [15] program. Typical Fourier transformation magnitude of the EXAFS data measured at 575 K around the Sr and Pd K-edges. The Fourier transformation magnitudes were fit using a classical shell-by-shell procedure using the Artemis program [15] based on the IFEFFIT code [16]. Theoretical backscattering amplitude and phase-shift functions used in the fitting procedure were calculated by the FEFF code [17].

2.2.3. Mössbauer spectroscopy

The Pd local structure was further studied. Pd was chemically substituted, by 5%, with natural abundant Fe and a ^{57}Fe Mössbauer spectrum in transmission geometry was collected at 295 K using a spectrometer equipped with a sinusoidal velocity transducer utilizing a $^{57}\text{Co}(\text{Rh})$ source. The velocity calibration was carried out using an $\alpha\text{-Fe}$ foil at the same temperature. The Mössbauer spectrum was fitted using the Mosswin 4.0 program [18].

2.2.4. Magnetometry/calorimetry/resistivity

Magnetometry measurements were carried out between 10 and 250 K utilizing a SQUID located in an MPMS-5S system. Calorimetry measurements were carried out between 50 and 300 K utilizing the relaxation method [19] using a Versalab Cryogen-free Physical Property Measurement System. The dc electrical resistance of bar-like specimen with dimensions of $20 \times 2 \times 2 \text{ mm}^3$ was determined by the four point method. Current reversal was applied to eliminate potential thermoelectric effects. The resistivity measurements were performed in static air between 80 and 300 K in a custom made cryostat and between 300 and 700 K in a custom made oven.

3. Experimental results

3.1. X-ray diffraction

Fig. 1 shows the X-ray diffraction patterns measured on Sr_2PdO_3 and $\text{Sr}_2\text{Pd}_{0.95}\text{Fe}_{0.05}\text{O}_3$ at room temperature. All reflections in both compounds appear roughly at the same positions. A Le Bail refinement is carried out in both datasets. A typical Le Bail refinement and the

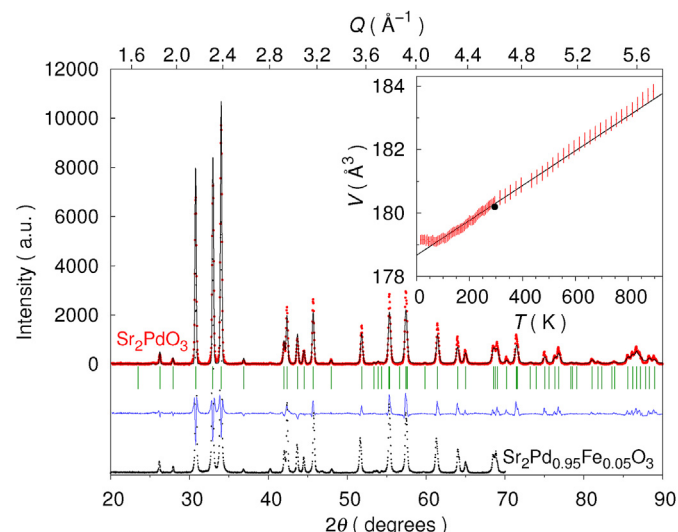


Fig. 1. Le Bail refinement (black line) of a typical diffraction pattern obtained by Sr_2PdO_3 (red points) and $\text{Sr}_2\text{Pd}_{0.95}\text{Fe}_{0.05}\text{O}_3$ (black points) using Cu K_α radiation at 295 K and the corresponding refinement residuals (blue line). The green vertical line designate the expected reflection positions. Inset shows the unit cell volume measured between 10 and 900 K on Sr_2PdO_3 (red points) and the 295 K volume measured on $\text{Sr}_2\text{Pd}_{0.95}\text{Fe}_{0.05}\text{O}_3$ (black point). The linear thermal expansion above 100 K is indicated by a black line. Typical errorbars are given. (For interpretation of the references to color in this figure legend, the reader is referred to the Web version of this article.)

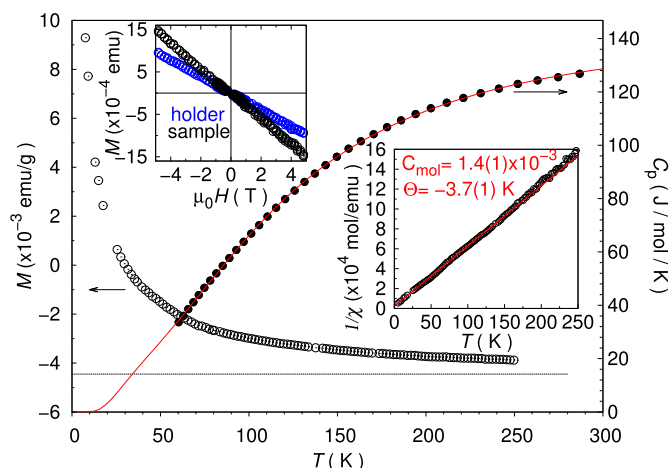


Fig. 2. (Left panel) Temperature dependence of magnetization measured on Sr_2PdO_3 under an applied magnetic field of 3 T. (Right panel) Heat capacity at constant pressure measured at zero magnetic field (black points) and the corresponding model (red line); see text. (Upper left inset) The field dependence of magnetization measured at 295 K for the empty sample holder and the sample holder loaded with the Sr_2PdO_3 sample. (Lower right inset) The temperature dependence of the molar magnetic susceptibility. Pointsize defines errorbar. (For interpretation of the references to color in this figure legend, the reader is referred to the Web version of this article.)

refinement residuals for the Sr_2PdO_3 data are also seen in Fig. 1. The extracted lattice parameters at room temperature are $a = 3.9782(3)\text{\AA}$, $b = 3.5313(3)\text{\AA}$, and $c = 12.824(1)\text{\AA}$ for Sr_2PdO_3 and $a = 3.9706(3)\text{\AA}$, $b = 3.5417(3)\text{\AA}$, and $c = 12.813(1)\text{\AA}$ for $\text{Sr}_2\text{Pd}_{0.95}\text{Fe}_{0.05}\text{O}_3$. The corresponding unit cell volume is given as an inset to Fig. 1. Sr_2PdO_3 and $\text{Sr}_2\text{Pd}_{0.95}\text{Fe}_{0.05}\text{O}_3$ have (within the experimental accuracy) the same unit cell volume at room temperature. A linear volumetric thermal expansion is observed in Sr_2PdO_3 between 100 and 900 K with a slope of $5475(122)\text{ pm}^3/\text{K}$.

3.2. Magnetometry

Fig. 2 shows the temperature dependence of magnetization measured between 10 and 250 K on Sr_2PdO_3 under an externally applied magnetic field of 3 T. A plot of the magnetization - applied magnetic field data at room temperature is shown as an inset to Fig. 2. The sample data have a steeper slope compared to the bare sample holder data. Sr_2PdO_3 appears to show a temperature dependent paramagnetic behaviour superimposed to a temperature independent core diamagnetism of $4.4 \cdot 10^{-3}\text{ emu/g}$. The inverse molar magnetic susceptibility extracted from these data is shown as inset to Fig. 2. The molar magnetic susceptibility of Sr_2PdO_3 appears to follow a Curie - Weiss law with $\Theta = -3.7(1)\text{ K}$ and a relatively low Curie constant, $C_{\text{mol}} = 1.4(1) \cdot 10^{-3}$.

3.3. Calorimetry

In addition Fig. 2 shows heat capacity data measured between 50 and 300 K. The heat capacity at room temperature is, about 130 J/mol/K , approaching the Dulong-Petit limit 150 J/mol/K in Sr_2PdO_3 . The heat capacity data were fitted using a Debye model superimposed with a collection of Einstein oscillators. The fitted curve is depicted in Fig. 2. The extracted Debye and Einstein temperature are $512(6)\text{ K}$ and $114(12)\text{ K}$, respectively. Moreover, the Einstein oscillators contribute by 19% in the total heat capacity.

3.4. Mössbauer spectroscopy

The Mössbauer spectrum measured with a Doppler velocity between

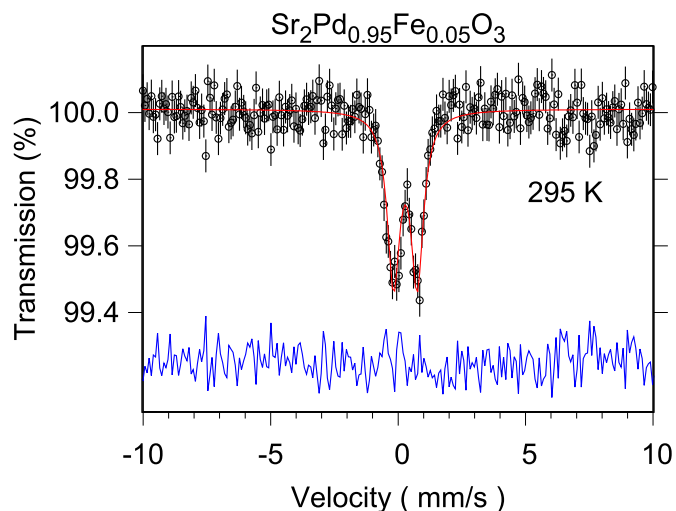


Fig. 3. ^{57}Fe -Mössbauer spectrum (black points) measured on $\text{Sr}_2\text{Pd}_{0.95}\text{Fe}_{0.05}\text{O}_3$ at 295 K, the corresponding model (red line), and the residuals (blue line). The velocity calibration was carried out using an $\alpha\text{-Fe}$ foil at room temperature. Typical errorbars are given. (For interpretation of the references to color in this figure legend, the reader is referred to the Web version of this article.)

-10 and 10 mm/s on $\text{Sr}_2\text{Pd}_{0.95}\text{Fe}_{0.05}\text{O}_3$ at 295 K is shown in Fig. 3. The nuclear absorption is reasonably low, less than 1%, given the low iron content and the low natural abundance of ^{57}Fe in Fe. Nevertheless, the obtained Mössbauer spectrum clearly shows a rather sharp doublet indicating that iron is located in a single site. The extracted isomer shift is $0.29(2)\text{ mm/s}$ and the quadrupole splitting is $0.93(3)\text{ mm/s}$ whereas the instrumental linewidth is $0.58(3)\text{ mm/s}$. No other contribution relevant to metallic iron or iron oxides which could result in a sextet or larger splitting is seen in the spectrum.

3.5. X-ray absorption

Figs. 4 and 5 show the measured X-ray Absorption Near Edge Structure (XANES) spectra after normalization around the Sr and the Pd K-edge, respectively, and its derivative at the lowest and highest measured temperature. A shoulder at 16115 eV and a peak at 16123 eV is observed in the near edge part of the Sr absorption spectrum. Similarly

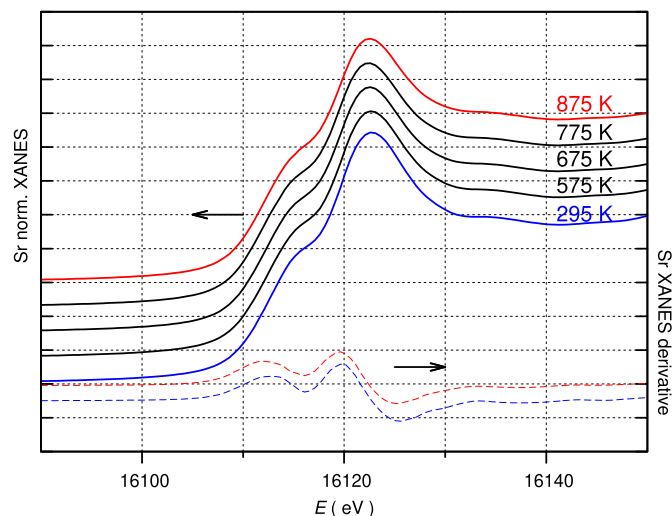


Fig. 4. X-ray Absorption Near Edge Structure (XANES) spectra measured on Sr_2PdO_3 around the Sr K-edge (solid line) upon heating up to 875 K. The XANES spectra are equally shifted vertically for clarity.

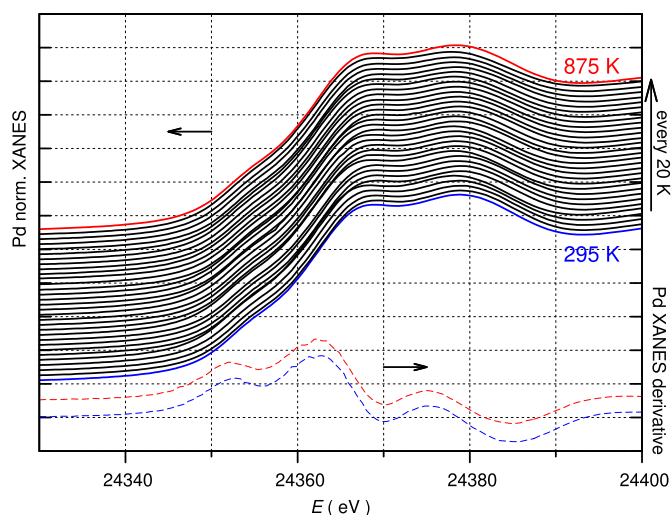


Fig. 5. X-ray Absorption Near Edge Structure (XANES) spectra measured on Sr_2PdO_3 around the Pd K-edge (solid line) and its derivative (dashed line) upon heating up to 875 K. The XANES spectra are equally shifted vertically for clarity.

a shoulder is observed at 24356 eV and two peaks at 24367 eV and 24378 eV in the near edge part of the Pd absorption spectrum. The relative intensity as well as the position of the observed features both in the Sr and Pd XANES do not change at elevated temperatures as is clearly indicated both in the actual data as well as the representative derivatives depicted in the same figures.

The crystal structure of Sr_2PdO_3 indicates that from Pd point of view there are two independent closely overlapping oxygens and a Sr cell, whereas from Sr perspective there are three independent Sr - O pairs and a Pd cell. The distance and the effective pair distribution parameters of Sr as seen from Pd and of Pd as seen from Sr are identical and thus kept the same in the refinement carried out in this study. Fitting all the remaining scattering paths independently would still result in a high number of variables due to the rather low local symmetry. In order to reduce the number of independent variables we assume that different oxygens will have similar distance changes and distribution, *i.e.*, Debye - Waller factor. A typical fit of the Fourier transformation magnitude, which involves a non-zero third cumulant, between 1 and 3.5 Å is shown in Fig. 6. The main features of the Fourier transformation magnitude are captured by the fit while the minor features within the fitting window are mainly attributed to termination errors of the Fourier transformation.

The EXAFS extracted Debye - Waller factors are shown as an inset in Fig. 6. The Pd - O pair has the lowest thermal displacement slope with temperature which indicates that the Pd - O bond is the stiffest while the Sr - O pair shows the steepest thermal displacement slope with temperature which indicates that the Sr - O bond is the weakest.

3.6. Resistivity

The electrical resistivity between 80 and 700 K measured on Sr_2PdO_3 in static air is shown in Fig. 7. A data gap observed in Fig. 7 around room temperature is related to the experimental setup exchange. The electrical resistivity shows a semiconducting behaviour in the measured temperature range. A systematic reduction of resistivity is observed upon thermal cycling. The temperature dependence of the initially measured resistivity curves, A and B, is fitted using a variable range hopping model, $\ln \rho = (E_0/kT)^{1/(d+1)} + \ln \rho_0$ [20], see inset to Fig. 7. The parameter d is related with the dimensionality of the system. Electrical transport in Sr_2PdO_3 is expected to take place predominantly along the corner sharing PdO_4 squares extending as 1D chains along the b axis on the $a - b$ crystallographic plane. As a result, the use of the

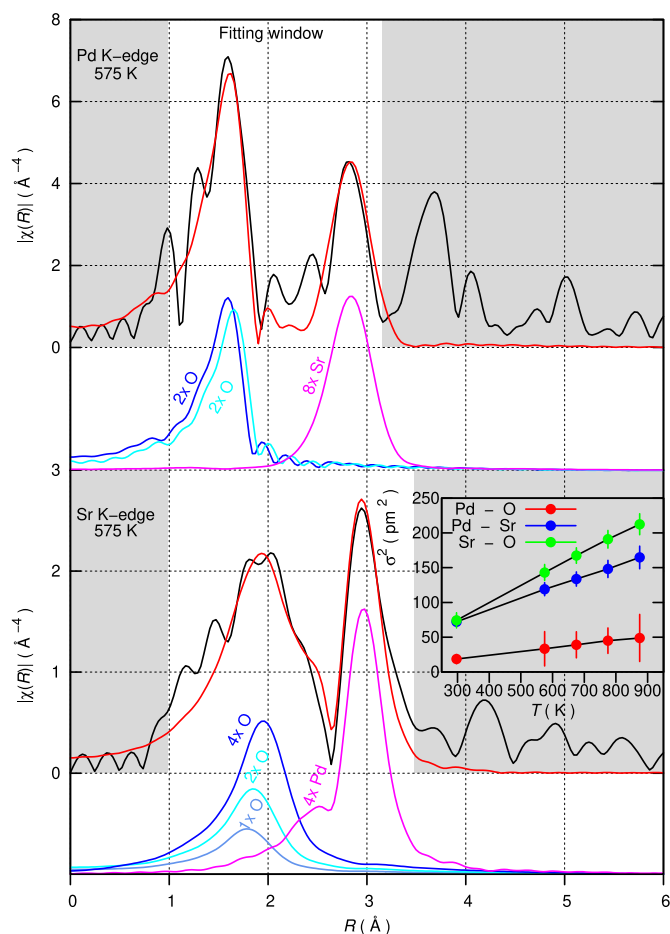


Fig. 6. Typical Sr K-edge (lower panel) and Pd K-edge (higher panel) Extended X-ray Absorption Fine Structure (EXAFS) measured on Sr_2PdO_3 at 575 K (Fourier transformation magnitude: black line), the best fit (red line) between 1 and 3.5 Å and the components used (color line); see text. Inset: The temperature dependence of the Debye - Waller factors between 300 and 900 K for the Pd - O (red), the Pd - Sr (blue), and the Sr - O (green) pairs extracted from the EXAFS analysis; lines between points are given as a guide for the eye. (For interpretation of the references to color in this figure legend, the reader is referred to the Web version of this article.)

variable range hopping model with $d = 1$ is justified. This model fits indeed the initially obtained resistivity curves satisfactorily. The extracted values for E_0 and ρ_0 are 11.3(1) meV and 7.59(1) Ohm cm in curve A, 9.32(1) meV and 4.33(1) Ohm cm in curve B. Both E_0 and ρ_0 decrease upon thermal cycling. Moreover, a notable deviation from the variable range hopping model starts to appear. The variable range hopping does not fit satisfactorily the consecutively measured electrical resistivity curve C which seems to conform better to an Arrhenius law, $\ln \rho = (E_1/kT) + \ln \rho_0$, see inset to Fig. 7. The extracted values for E_1 and ρ_0 are 3.2(1) meV and 3.09(1) Ohm cm in curve C.

4. Discussion

The successful chemical substitution of Pd with 5% Fe in Sr_2PdO_3 is verified by the absence of spurious reflections, which indicates absence of long range ordered impurity phases, in the obtained X-ray diffraction patterns as well as by the absence of a second component in the measured Mössbauer spectrum, which indicates absence of amorphous impurity phases. The measured isomer shift in Sr_2PdO_3 at room temperature is, 0.29(2) mm/s, in good agreement with the one measured in Sr_2FeO_3 [10], which is about 0.30 mm/s. Such values are typical for Fe^{2+} in square coordination [21]. The quadrupole splitting in Sr_2PdO_3

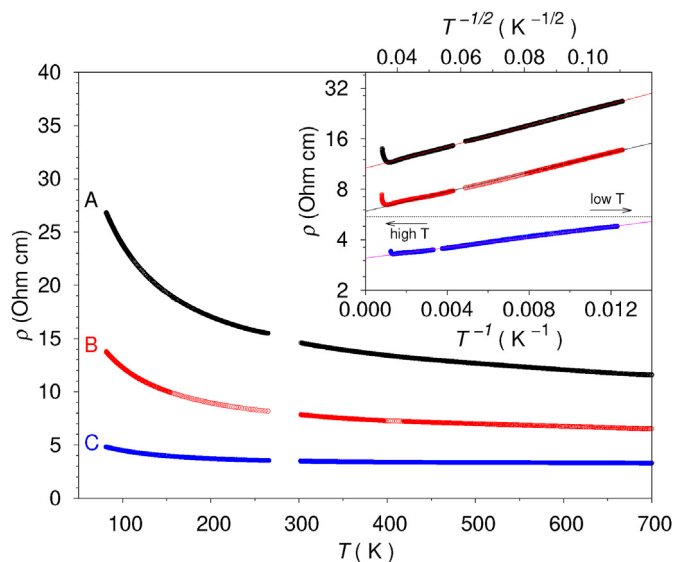


Fig. 7. Electrical resistivity between 80 and 700 K measured consequently (curves: A, B, C) on the same Sr_2PdO_3 sample in static air. Inset: (upper panel) the curves A and B plotted in the variable range hopping configuration with $d = 1$. (lower panel) the curve C plotted in the Arrhenius configuration; see text. The high temperature and the low temperature regime is indicated for clarity.

is, $0.93(3)$ mm/s, notably less compared with the corresponding in Sr_2FeO_3 [10], 1.33 mm/s. An electric field gradient at the Pd site, eq , can be calculated from the measured quadrupole splitting, dE , using the formula: $dE = e \cdot eq \cdot Q/2$, where e is the electron charge, Q is the nuclear quadrupole moment of the excited state which for ^{57}Fe is $0.15(2)$ b [22]. As a result the electric field gradient at the Pd site at room temperature is $eq = 5.9(1) \cdot 10^{17}$ V/cm². The electric field gradient is usually correlated with the local atomic structure. The quadrupole splitting at the transition metal site in Sr_2PdO_3 is smaller than the corresponding in Sr_2FeO_3 , thus, the PdO_4 square planar coordination in Sr_2PdO_3 is expected to be more symmetric compared to the FeO_4 square planar coordination in Sr_2FeO_3 .

No magnetic ordering in the measured temperature range is observed in this study in Sr_2PdO_3 , whereas, both in the isostructural Sr_2CuO_3 and Sr_2FeO_3 an antiferromagnetic transition is observed at about 5 and 180 K, respectively. Nevertheless, the peculiar magnetic state which shows a Curie-paramagnetic susceptibility indicating antiferromagnetic interactions superimposed to a core diamagnetic state similarly to Ref. [11,23] is confirmed. Thus, it becomes clear that a chemical substitution of Pd with other transition metals, *i.e.*, Fe or Cu, in Sr_2PdO_3 provides the means to fine tune its properties to a great extent.

The heat capacity data obtained in this study could not be fitted using a Debye model alone. Only after the introduction of a collection of Einstein oscillators [24] the fitting curve described the experimental data satisfactorily. The extracted Einstein temperature, $114(12)$ K, indicates that the Debye model breaks around $10(1)$ meV. Such a break in the Debye model could be related to a van-Hove singularity close to the edge of the Brillouin zone, to localized optical modes, or to a peculiar electronic contribution in heat capacity. To the best of our knowledge, no first principle vibrational calculations exist in literature to clarify the existence of a van-Hove singularity or localized optical modes at this energy range. Such a collection of Einstein oscillators extracted from our heat capacity measurements is expected to have an impact in the thermal transport of Sr_2PdO_3 . To the best of our knowledge heat conductivity measurements are also not available in the literature for Sr_2PdO_3 , however, such measurements exist for the isostructural Sr_2CuO_3 [25] and show an anomalously enhanced thermal conductivity

above 40 K. Whether such an anomaly in thermal conductivity is related with spin excitations; with localized vibrational modes; or with an electronic mechanism found in this study remains indeed an interesting open question.

The volume thermal expansion coefficient, α_V , at room temperature could be estimated by normalizing the slope of the unit cell volume, $5475(122)$ pm³/K, extracted from temperature dependent X-ray diffraction patterns to the unit cell volume at room temperature. The estimated thermal expansion coefficient at room temperature is $3.0(1) \cdot 10^{-5}$ K⁻¹.

The macroscopic Grüneisen parameter, γ , which quantifies the degree of anharmonicity could be extracted using the volume thermal expansion coefficient, the heat capacity at constant volume, C_V , and the isothermal compressibility, K_T by $\gamma = \alpha_V/(C_V K_T)$. At room temperature the volume thermal expansion coefficient and the heat capacity extracted from this study is $\alpha_V = 3.0(1) \cdot 10^{-5}$ K⁻¹ and $C_V \approx C_P = 127$ J/mol/K, respectively. Isothermal compressibility, K_T , was not measured in this study but it can be extracted from high pressure X-ray diffraction literature data [12], $K_T = 1.01$ Mbar⁻¹. As a result the macroscopic Grüneisen parameter is $\gamma = 2.5(1)$. The extracted value for the macroscopic Grüneisen parameter in Sr_2PdO_3 at room temperature is close to the Grüneisen parameter of simple metals [26], $\gamma \approx 2$.

The EXAFS extracted Debye - Waller factors include a static contribution relevant to the crystal structure imperfections and a dynamical contribution relevant to the thermal displacement. A pure linear increase with temperature is observed in the EXAFS extracted atomic displacement parameters for the Sr - O, Pd - O, and Sr - Pd pairs. The difference in slopes observed for the different pairs indicate that the main contribution in the extracted Debye - Waller factors is dynamic. Moreover, the pure linear increase of the atomic displacement parameters according to the equi-partition theorem indicates that the harmonic approximation can be fully justified. Thus, both from microscopic and macroscopic point of view anharmonic effects are not expected to play an important role in Sr_2PdO_3 .

No change is observed in our XANES spectra both for Pd and Sr, thus, a potential valence change for both Pd and Sr at elevated temperatures can be safely excluded.

An effect relevant to electrical resistivity, which can be attributed neither to anharmonicity nor to a potential valence change of the cations, is puzzling. The electrical resistivity in Sr_2PdO_3 between 80 and 700 K shows a semiconducting behaviour, see Fig. 7. A systematic reduction in electrical resistivity is observed upon thermal cycling. The observed thermal dependence of resistivity satisfies the 1D variable range hopping model suggesting that the carriers are localized within the chains and hop with a thermal activation energy of about 10 meV which is comparable to the Einstein energy obtained from the heat capacity analysis. The good match between the energy of the Einstein oscillators obtained from the heat capacity analysis and the thermal activation energy extracted from the analysis of the electrical resistivity data suggests that a peculiar electronic contribution is involved in the system. The decrease of E_0 and ρ_0 upon thermal cycling indicates delocalization of carriers. As delocalization proceeds, hopping between nearest neighbours within the $a - b$ crystallographic plane finally dominates resulting in 3D band conduction described by an Arrhenius law. However, the origin of delocalization is not quite clear for us. Sr_2PdO_3 is not known to accept O₂-excess like its isostructural $\text{Sr}_2\text{CuO}_{3+x}$ counterpart, or the archetypal $\text{La}_2\text{CuO}_{4+x}$. Moreover this would require the existence of higher valence states of Pd, which is excluded by our XANES data. Therefore O₂ exchange with the environment as the origin of delocalization is not probable. Tentatively we believe that delocalization of carriers originates in thermally induced redistribution of oxygen atoms from the apical sites to the PdO_4 conducting planes, (as known for $\text{Sr}_2\text{CuO}_{3+x}$) where they act as dopants affecting greatly the electrical properties of the system.

5. Conclusion

In summary, we have synthesized by a modified solid state reaction bulk Sr_2PdO_3 and we have carried out a combined microscopic and macroscopic experimental characterization. We report no structural transition between 10 and 900 K, and no valence change for both Sr and Pd up to 900 K. A Curie-paramagnetic susceptibility indicating anti-ferromagnetic interactions superimposed to a core diamagnetic state is confirmed. A collection of Einstein oscillators is involved in thermal transport. A moderate anharmonicity is identified and quantified in a macroscopic Grüneisen parameter of 2.5(1) at room temperature. Finally we report a systematic reduction in electrical resistivity and a change in the conduction mechanism upon thermal cycling which suggests that a peculiar electronic mechanism is involved.

Acknowledgements

Dr. R. Ruffer is acknowledged for provision of the starting materials. The European Synchrotron Radiation Facility is acknowledged for XAS beamtime provision at BM23. D.B acknowledges financial support from the Industrial Partnership Program (IPP-I28) of Foundation for Fundamental Research on Matter (FOM) (The Netherlands) and BASF New Business. The technical support of Mr. A. Lefering is acknowledged during the magnetometry measurements.

References

- [1] E. Dagotto, Correlated electrons in high-temperature superconductors, *Rev. Mod. Phys.* 66 (1994) 763–840.
- [2] G. Shirane, R. Birgeneau, Y. Endoh, M. Kastner, Spin fluctuations in insulating, weakly metallic and superconducting $\text{La}_{2-x}\text{Sr}_x\text{CuO}_4$, *Physica B* 197 (1) (1994) 158–174.
- [3] Y. Maeno, H. Hashimoto, K. Yoshida, S. Nishizaki, T. Fujita, J.G. Bednorz, F. Lichtenberg, Superconductivity in a layered perovskite without copper, *Nature* 376 (6506) (1994) 532–534.
- [4] B.J. Kim, H. Jin, S.J. Moon, J.-Y. Kim, B.-G. Park, C.S. Leem, J. Yu, T.W. Noh, C. Kim, S.-J. Oh, J.-H. Park, V. Durairaj, G. Cao, E. Rotenberg, Novel $J_{\text{eff}} = 1/2$ mott state induced by relativistic spin-orbit coupling in Sr_2IrO_4 , *Phys. Rev. Lett.* 101 (2008) 076402.
- [5] J. Kim, D. Casa, M.H. Upton, T. Gog, Y.-J. Kim, J.F. Mitchell, M. van Veenendaal, M. Daghofer, J. van den Brink, G. Khaliullin, B.J. Kim, Magnetic excitation spectra of Sr_2IrO_4 probed by resonant inelastic x-ray scattering: establishing links to cuprate superconductors, *Phys. Rev. Lett.* 108 (2012) 177003.
- [6] A. Georges, L. de Medici, J. Mravlje, Strong correlations from Hund's coupling, *Ann. Rev. Condens. Matter. Phys.* 4 (1) (2013) 137–178.
- [7] D.I. Khomskii, *Transition Metal Compounds*, Cambridge University Press, 2014.
- [8] M. Hoesch, P. Piekarz, A. Bosak, M. Le Tacon, M. Krisch, A. Kozłowski, A.M. Oleś, K. Parlinski, Anharmonicity due to electron-phonon coupling in magnetite, *Phys. Rev. Lett.* 110 (2013) 207204.
- [9] T. Ami, M.K. Crawford, R.L. Harlow, Z.R. Wang, D.C. Johnston, Q. Huang, R.W. Erwin, Magnetic susceptibility and low-temperature structure of the linear chain cuprate Sr_2CuO_3 , *Phys. Rev. B* 51 (1995) 5994–6001.
- [10] C. Tassel, L. Seinberg, N. Hayashi, S. Ganesanpotti, Y. Ajiro, Y. Kobayashi, H. Kageyama, Sr_2FeO_3 with stacked infinite chains of FeO_4 square planes, *Inorg. Chem.* 52 (10) (2013) 6096–6102.
- [11] Y. Nagata, T. Taniguchi, G. Tanaka, M. Satho, H. Samata, Magnetic properties of $\text{Sr}_2\text{Pd}_{1-x}\text{M}_x\text{O}_3$ (M=Co, Cu), *J. Alloy. Comp.* 346 (1) (2002) 50–56.
- [12] T. Yamamoto, Y. Kobayashi, T. Okada, T. Yagi, T. Kawakami, C. Tassel, S. Kawasaki, N. Abe, K. Niwa, T. Kikegawa, N. Hirao, M. Takano, H. Kageyama, B1-to-B2 structural transitions in rock salt intergrowth structures, *Inorg. Chem.* 50 (22) (2011) 11787–11794.
- [13] E.H. El-Ads, A. Galal, N.F. Atta, The effect of a-site doping in a strontium palladium perovskite and its applications for non-enzymatic glucose sensing, *RSC Adv.* 6 (2016) 16183–16196.
- [14] O. Mathon, A. Beteva, J. Borrel, D. Bugnazet, S. Gatla, R. Hino, I. Kantor, T. Mairs, M. Munoz, S. Pasternak, F. Perrin, S. Pascarelli, The time-resolved and extreme conditions XAS (Texas) facility at the european synchrotron radiation facility: the general-purpose EXAFS bending-magnet beamline BM23, *J. Synchrotron Radiat.* 22 (2015) 1548–1554.
- [15] B. Ravel, M. Newville, *ATHENA, ARTEMIS, HEPHAESTUS*: data analysis for X-ray absorption spectroscopy using *IFEFFIT*, *J. Synchrotron Radiat.* 12 (4) (2005) 537–541.
- [16] M. Newville, *IFEFFIT*: interactive XAFS analysis and feff fitting, *J. Synchrotron Radiat.* 8 (2) (2001) 322–324.
- [17] A.L. Ankudinov, J.J. Rehr, Development of XAFS theory, *J. Synchrotron Radiat.* 10 (5) (2003) 366–368.
- [18] Z. Klencsár, Mosswin—methodological advances in the field of Mössbauer data analysis, *Hyperfine Interact.* 217 (1) (2013) 117–126.
- [19] J.S. Hwang, K.J. Lin, C. Tien, Measurement of heat capacity by fitting the whole temperature response of a heat-pulse calorimeter, *Rev. Sci. Instrum.* 68 (1) (1997) 94–101.
- [20] N.F. Mott, E.A. Davis, *Electronic Processes in Non-crystalline Materials*, Oxford University Press, 1979.
- [21] Y. Tsujimoto, C. Tassel, N. Hayashi, T. Watanabe, H. Kageyama, K. Yoshimura, M. Takano, M. Ceretti, C. Ritter, W. Paulus, Infinite-layer iron oxide with a square-planar coordination, *Nature* 450 (2007) 1062.
- [22] G. Martínez-Pinedo, P. Schwerdtfeger, E. Caurier, K. Langanke, W. Nazarewicz, T. Söhnel, Nuclear quadrupole moment of ^{57}Fe from microscopic nuclear and atomic calculations, *Phys. Rev. Lett.* 87 (2001) 062701.
- [23] K.M. Kojima, J. Yamanobe, H. Eisaki, S. Uchida, Y. Fudamoto, I.M. Gat, M.I. Larkin, A. Savici, Y.J. Uemura, P.P. Kyriakou, M.T. Rovers, G.M. Luke, Site-dilution in the quasi-one-dimensional antiferromagnet $\text{Sr}_2\text{Cu}_{1-x}\text{Pd}_x\text{O}_3$: reduction of Néel temperature and spatial distribution of ordered moment sizes, *Phys. Rev. B* 70 (2004) 094402.
- [24] R.P. Hermann, F. Grandjean, G.J. Long, Einstein oscillators that impede thermal transport, *Am. J. Phys.* 73 (2) (2005) 110–118.
- [25] A.V. Sologubenko, K. Giannò, H.R. Ott, A. Vietkine, A. Revcolevschi, Heat transport by lattice and spin excitations in the spin-chain compounds SrCuO_2 and Sr_2CuO_3 , *Phys. Rev. B* 64 (2001) 054412.
- [26] M. Hasegawa, W.H. Young, Grüneisen parameters for simple metals, *J. Phys. F Met. Phys.* 10 (2) (1980) 225.